A Simulation Study of Ion Concentration, Electric Potential and Ion Current within Nation

Wesley Gould and Philip Taylor

Case Western Reserve University, Department of Physics

Abstract

The results of a Monte Carlo molecular simulation of a single pore Nafion are presented, showing the concentration of ions within a pore, the electric potential inside the pore, and an estimate of the ion current as a function of the pore construction with various applied external fields. The ion concentration and electric potential measurements are then compared with existing theoretical models by Berg and Pintauro. The ion current is measured and comparisons are made with several other research groups. Further analysis shows that it is insufficient to treat the sulfonates as a smeared charge rather than as discrete elements. Ion current is presented as a function of the water content and pore radius, which should be proportional to the conductivity as a function of those parameters.

I. INTRODUCTION

Virtually all internal combustion engines are designed to utilize fossil fuels as an energy source. Heavy reliance on these engines in vehicles directly results in great demand for these fuels, which are not replenished at anywhere near the rate at which they are being used. Furthermore, many studies have suggested that the byproducts of these engines, such as carbon dioxide, may cause changes to the climate and global weather patterns. However, there are few solutions to replacing the internal combustion engines that we use today. Of those, all have severe limitations that could prevent them from becoming viable. One possible solution, for example, is the use of rechargeable electric vehicles. These, however, have problems with range and charging time. An unbreakable dependence on fossil fuels is thus a severe problem for modernized societies wishing to reduce their carbon footprints and dealing with ever shrinking reserves of fuels.

PEM (Polymer Electrolyte Membrane) fuel cells are capable of utilizing hydrogen as a fuel, which can be produced chemically from fossil fuels or from water via electrolysis. This allows for a wide variety of energy sources to be used to make the hydrogen fuel and allow users to abstract the operation of an automobile from the source of the fuel, thus allowing a seamless transition into a lower carbon world.

PEM fuel cells typically consist of several components. Fuel in the form of diatomic hydrogen is exposed to a platinum catalyst. The hydrogen attaches itself to the platinum catalyst and is able to move in a monatomic state. Adjacent to the platinum catalyst is a membrane which is a strong acid and is permeable to protons but not un-ionized hydrogen. After passing through the membrane, the protons are exposed to oxygen, typically on another platinum catalyst, and react readily. Given that the electrons have remained on the platinum catalyst with which the hydrogen first came into contact, a potential difference forms between the two catalysts. This can be used to power electrical devices.

This paper is concerned with the membrane, and in particular, the most widely-used material, Nafion[1]. Nafion has a backbone chain of polytetrafluroethylene and branches that terminate in sulfonate groups, SO_3. In its acid form, the negatively charged sulfonates combine with protons. These protons dissociate in the presence of water and then provide the mobile ions that transport electrical charge.

Over the years, several groups have discussed the structure of Nafion and the distribu-

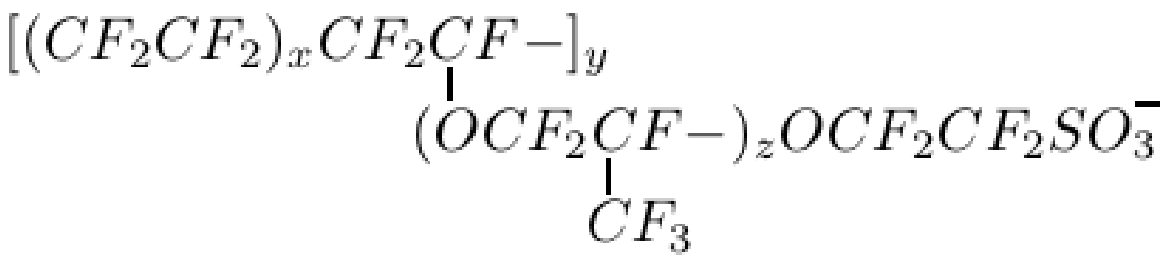

FIG. 1: A chemical diagram of Nafion^{TM}, where x, y, and z vary based on the preparation of the membrane

tion of protons within it. The earliest model of Nafion's^{TM}structure was the core-shell model suggested by Fujimura *et al.*.[2] Their model, however, did not sufficiently explain the transport properties, and so other models were developed[3]. Gierke and Hsu proposed a cluster network model in which spherical hydrophobic clusters lined on the inside with sulfonates are connected by small channels also lined with sulfonates[4]. Schmidt-Rohr and Chen proposed the water-channel model in 2008, in which Nafion has a large number of hydrophilic, parallel, cylindrical pores lined with sulfonate groups that are attached to the side chains of the Nafion[5]. In the water-channel model, the conduction of protons occurs along the interior surface of approximately cylindrical pores.

For the purposes of this paper, several variations on the water-channel model are used to represent Nafion. Other models are not explored, not to make a statement about their correctness, but because the authors felt that a more focused work would have more depth and therefore be of better use to other researchers than a less focused work that explored several Nafion models.

Several groups have worked on the electric potential and ion concentration within Nafion. Bontha and Pintauro considered the electric potential within an approximately cylindrical pore[6]. It is worth noting however that Bontha and Pintauro did not find exact solutions, but rather numerical ones, and that they approximated the walls of the cylindrical pore as planes. Berg and Ladipo did find exact solutions for both the ion concentration and the electric potential within an infinite cylindrical pore of Nafion^{TM}, but they do admit that their exact solutions are based on assumptions such as treating ions as a continuous medium, that may not be true on very small scales.[7] Furthermore, they admit possible inaccuracies if there is a net flux present, as there will be in a PEM fuel cell. This work will attempt to

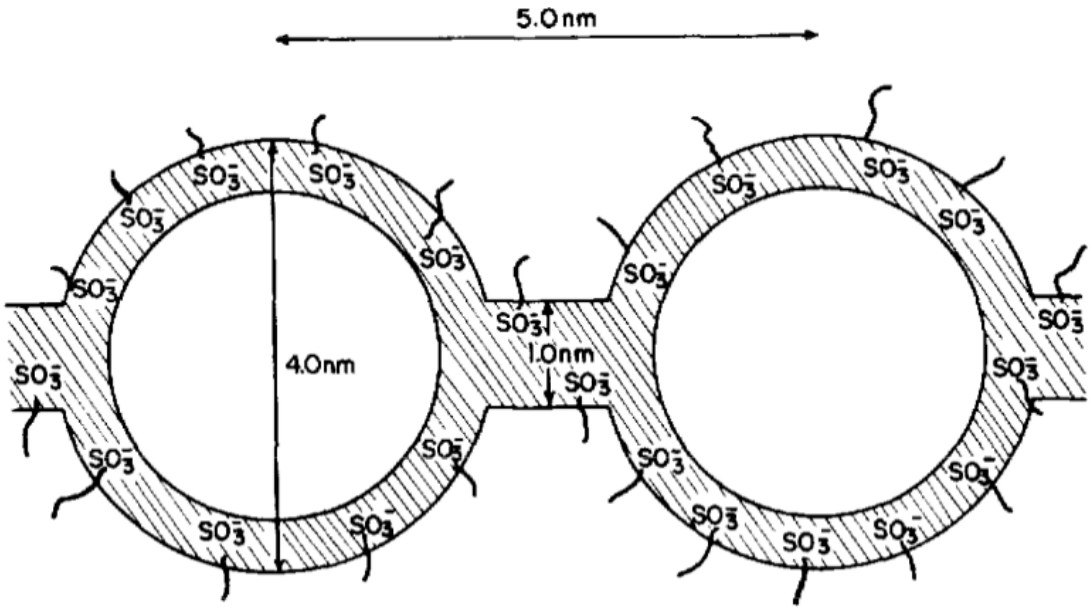

FIG. 2: The cluster-network model of Nafion, image courtesy Gierke and Hsu[4]. Notice the side chains ending in sulfonate groups protruding from the approximately spherical clusters of backbone material.

address these concerns about approximations by utilizing simulations of an approximately cylindrical pore on the molecular level.

II. MODEL

A. Representation of Molecules

Schmidt-Rohr and Chen showed that at 20 vol% water, Nafion pores had, on average, a diameter of approximately 2.4 nm[5]. Consequently, pores with diameters of 2, 3, and 4 nm were simulated, which were comparable with the diameters found in other studies (citations go here). The pore was modeled as an infinite length cylinder, which was a reasonable approximation for a pore in the water channel model (more citations). Because a typical membrane is very thick as compared to the diameter of the pores, the membrane is modelled as having an infinite length by use of periodic boundary conditions[8].

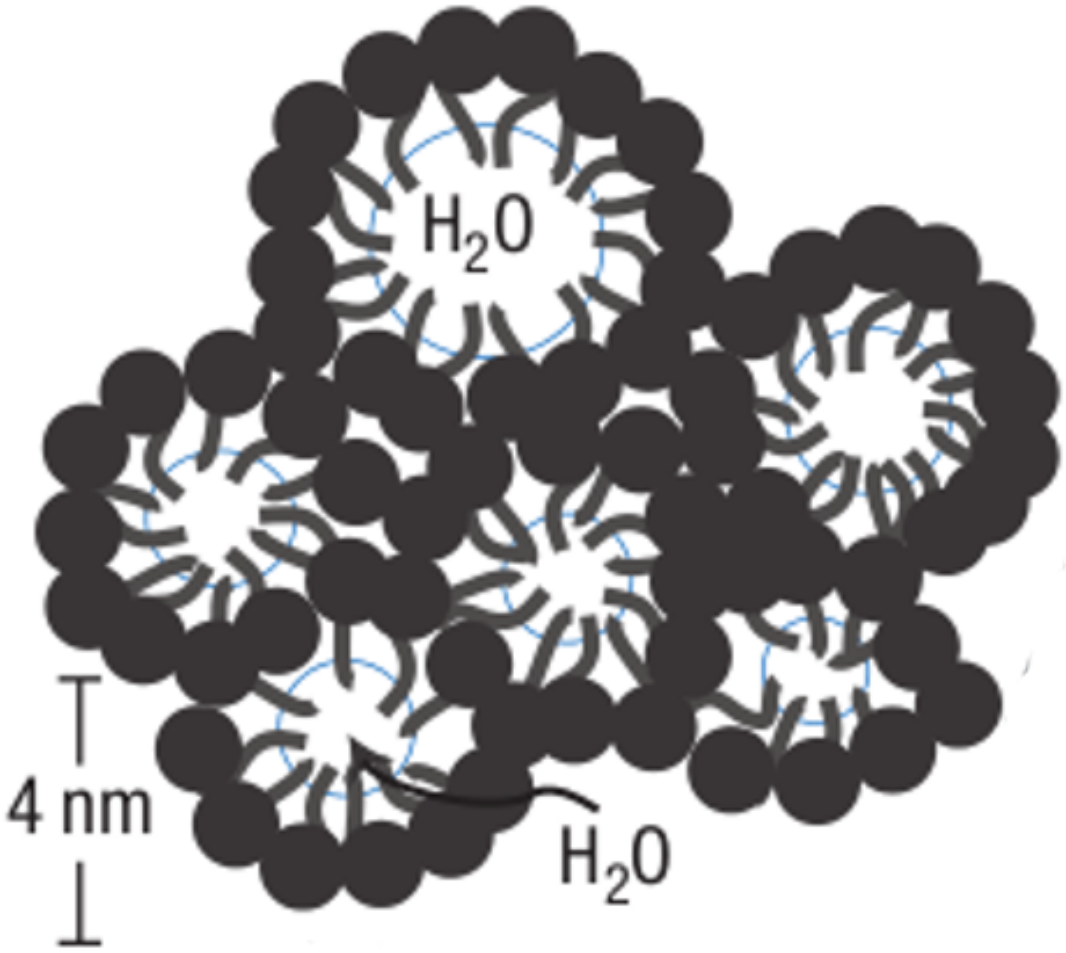

FIG. 3: The water channel model of Nafion, image courtesy Schmidt-Rohr and Chen[5]. Notice the circles representing the approximately cylindrical pores formed by hydrophobic backbone.

Several models were used to represent the side chains, with varying degrees of accuracy and computational difficulty. The first model is the simplest, which is to model the sulfonates as a uniformly smeared charge and then note that due to Gauss's law, the field inside of the pore due to the sulfonates is zero. This model is used, not because it is accurate, but because it is the closest to what Pintauro and Berg used.

The second model is to assume that the sulfonates are fixed point charges that never move, and have some volume, as represented by a Lennard-Jones potential. These sulfonate groups were given a charge -1e, and were fixed in place on a triangular lattice grid, with a

separation distance of 0.8 nm. This model does not incorporate the flexing of side chains and simply represents the side chains as these singular points. While this may not be a completely accurate picture of Nafion, it is plausible that the flexing of the side chains will have little effect on the properties of the system, and is still more accurate than the analytical studies because the sulfonate groups are represented as discrete points rather than as a continuous distribution[6,7].

The third and most accurate model examined treated the side chains as a series of linked polymer sections. This model was the same as the one used by Allahyarov and Taylor, where subsections of the sidechains are given three internal potentials to govern their motion: one for bond length, one for bond angle, and one for the dihedral angle[9]. The ends of the side chains were anchored again on a fixed lattice grid on a cylindrical surface, but the cylindrical surface used to anchor the side chains was larger than the walls of the system by 80% of the expected side chain length, such that a small section protruded into the cylinder, to be comparable to the other sulfonate models with regard to the placement of the sulfonate groups.

Water was simulated using the TIP3P model of water[10] in which the neutral molecule of H_2O is represented as 3 individual point charges. There is a net charge of, -0.82e on the oxygen atom and $+0.41$e on each hydrogen atom, such that the net charge of the water molecule is zero and it possesses a net dipole moment of 2.35 Debyes. Pairwise Coulombic potentials are evaluated using these assigned charges. Additionally, pairwise Lennard-Jones potentials were also included between oxygen atoms to prevent the overlap of the molecules in the system.

Each free proton was assumed to form a hydronium complex in this simulation. The hydronium ions were given a $+1$e net charge and were present in the same quantity as the sulfonate groups such that the net charge of the system was zero. As with water the bond length and bond angle are kept fixed. The exact values for the bond lengths, bond angles, and charge magnitudes are the same used by Jang, *et al.*[11]

B. Interaction Potentials

Within the simulation, Lennard-Jones potentials and Coulombic potentials were both employed. The Coulombic potential between any two point charges is given by Coulomb's

law,

$$U_c(q_1, q_2, r) = \frac{q_1 q_2}{\epsilon_0 r} \tag{1}$$

where U_c is the Coulombic potential, ϵ_0 is the permittivity of free space, q_1 and q_2 are the amounts of charge at the two points, and r is the distance between them. It is important to note that a dielectric constant was not included in Coulomb's law because that is modelled using the TIP3P water molecules. Furthermore, a Lennard-Jones potential,

$$U_{LJ}(r) = 4\epsilon \left[\left(\frac{\sigma}{r}\right)^{12} - \left(\frac{\sigma}{r}\right)^{6} \right] \tag{2}$$

was included between any two, adjacent oxygen atoms. Here r is the distance between the oxygen atoms, and ϵ and σ are constants with values of $0.6364 KJ/mol$ and $0.31506 nm$ respectively. Also, the Lennard-Jones potential was only computed for oxygen atoms within 2.5σ of each other, and a constant value of -0.0163ϵ is added to all computations of the Lennard Jones potential in order to make the region near the cutoff of 2.5σ continuous.

III. METHODS

A. Metropolis Monte Carlo

MMC (Metropolis Monte Carlo) simulations were performed on this model. As in any other Metropolis Monte Carlo simulation, once the change in potential, ΔU, was computed for a given trial move, the probability, p, of accepting a trial move was given a Boltzmann factor,

$$p(r) = e^{-\beta \Delta U} \tag{3}$$

Both water and hydronium were allowed to translate and rotate freely in the trial moves. As a caveat, the simulation places a cap on the magnitude of trial moves. A set of simulations was first executed and used to calibrate the value for this upper limit, by varying its value until a desired acceptance rate of 20% was achieved. Afterwards, that cap was set to a fixed value for all simulations which was chosen based on the values observed across the calibration simulations.

In order to generate translational trial moves, a vector with three random components between -1 and 1 was created. If the magnitude of this vector was greater than 1, then a

new one was generated until one with a magnitude less than or equal to unity was found. This method ensures that all trial moves are chosen from a distribution that is uniform. The components of this vector are then multiplied by the scalar cap. Likewise, when a rotational trial move is generated, a lower limit was placed on the magnitude of the scalar product of the current orientation vector and the proposed orientation vector. The rotational trial move is also chosen from a uniform distribution, in a similar manner to the translational moves.

In order to set up the system initially, the sulfonate groups were placed in fixed positions along the edges of the cylindrical boundary. The hydronium ions and water molecules were then placed into the system at locations chosen randomly from a uniform distribution within the cylindrical boundaries, and were given random orientations. This procedure of randomizing the starting state avoids biasing the results of the simulation by placing the molecules in any predetermined ordering.

After the system was initially set up in this semi-random state, new states are generated repeatedly following the rules of Metropolis Monte Carlo simulations. As more states are generated, the molecules in the system will approach an equilibrium state. By plotting the potential energy of a sample system as a function of the number of time steps, it was observed that at least 10k iterations of the Metropolis algorithm were needed to equilibrate all of the systems being examined.

B. Ion Concentration and Electric Potential

Computing the ion concentration was a simple matter of generating bin counts of the number of hydronium ions as a function of position at each iteration that data were collected, and then dividing this histogram by the volume of the cylindrical shell that represents each bin, and then dividing again by the number of times that data was collected. This yielded a number that was the average number of hydronium ions in each bin, where the standard deviation was equal to the square root of the bin count divided by the volume of the bin and the number of iterations for which data was collected.

The algorithm for computing the electric potential was also similar in that it also makes use of bin-counts. The system was again divided into a number of bins and the charge of each point charge was added to the bin that it was located in. Then each bin also has the

sum of the contents all of the smaller radius bins added to it. This yields the net charge within a cylindrical shell of the same radius as the outermost edge of each bin. A simple application of Gauss's law yields the flux, which was proportional to the field because this system was assumed to be cylindrically symmetric. The field was then averaged over the many times that data was collected, and a mean is computed.

C. Conductivity Estimate

In order to get an estimate of the conductivity of the pores, an electric field was applied along the axis of the cylinder, and an estimate of the current was recorded. Using Ohm's law, this current estimate can be divided by the magnitude of the external field to give an estimate of the pore conductivity.. This applied field needed to be kept relatively small as compared to the other fields in the system, but as was shown separately by Pintauro and Berg, the magnitude of the radial field due to charges on the hydronium ions and sulfonates is typically on the order of 1 eV/nm, thus we predicted that fields smaller than this would yield accurate estimates of the ion current.

The current was estimated by simply counting the number of hydronium ions passing through the endcaps, incrementing a counter when molecules move parallel to the cylinder's axis, and decrementing the counter when they move antiparallel to it. After a large number of metropolis steps, this yields a number that is proportional to the ion current and to the number of metropolis steps for which data were collected. Dividing this resultant number by the number of metropolis steps and the magnitude of the field then yields an estimate for the conductivity of the pore which is proportional to the actual pore conductivity.

IV. RESULTS

A. Ion Concentration and Electric Potential

A pore was simulated for comparison with Berg's and Pintauro's results, with a radius of 1.10 nm, and $\lambda = 6$. $\lambda = 6$ was chosen because it is one typical value for the water content of Nafion. Shown in Figures 4 and 5 are the measured values for the ion concentration as a function of distance from the walls of the pore for our 3 models for the sulfonate side chains alongside the theory from Berg and the simulation results from Pintauro. It should be noted

that the values for Berg's theory were calculated using a dielectric constant of 1 because there is no water in these systems. The pore was equilibrated for 15k Metropolis steps and then ion concentration and electric potential were recorded for 15k more steps.

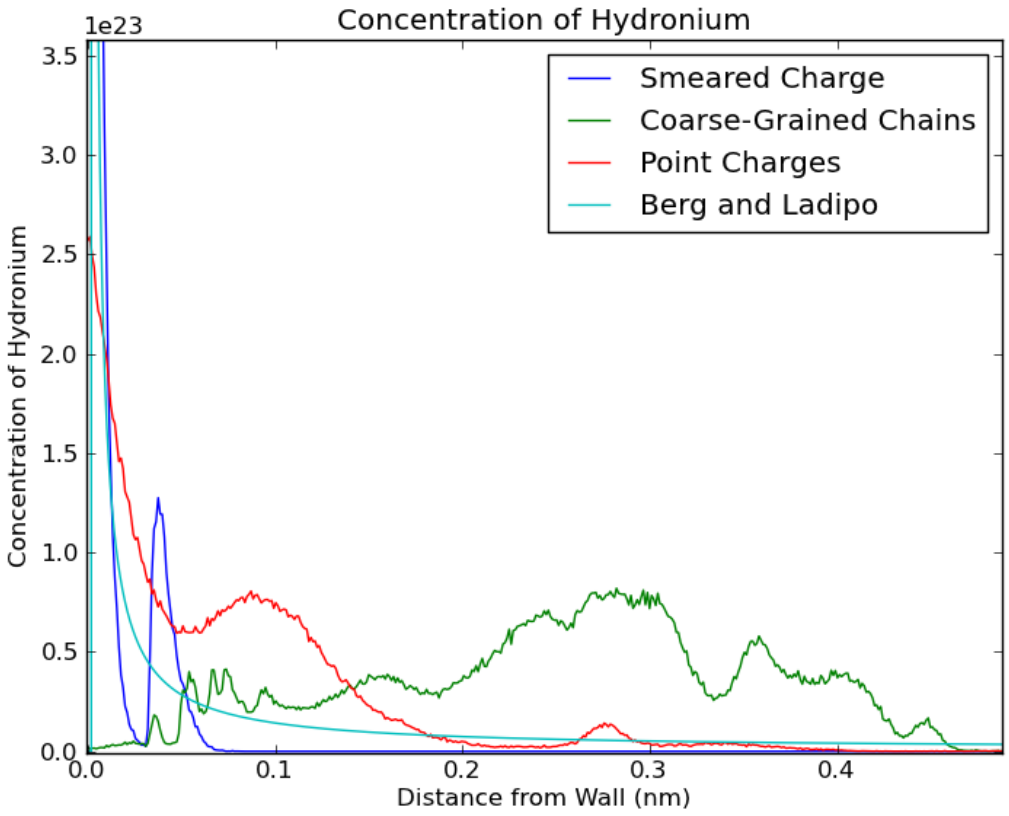

FIG. 4: Average concentration of hydronium ions as a function of distance from the pore walls for our 3 models, alongside the results from Berg

Several pores were simulated with varying radius and λ, and in those simulations the concentration of hydronium ions was recorded, as well as the electric potential. In particular pores of radius 1.10 nm, 1.32 nm 1.54 nm, 1.76nm, 1.98 nm and 2.20 nm were chosen, and were simulated with $\lambda = 6$. For these pores, no external electric field was applied. The values for the radius were chosen so that there would be no edge effects due to the triangular lattice, or rather, that there would be an integer number of triangles around the circumference with sulfonate groups at the vertices. λ was chosen to be 6 simply because it is a fairly typical value for a low hydration system. These simulations were each equilibrated for 15k metropolis steps and then the ion concentration and electric potential were recorded

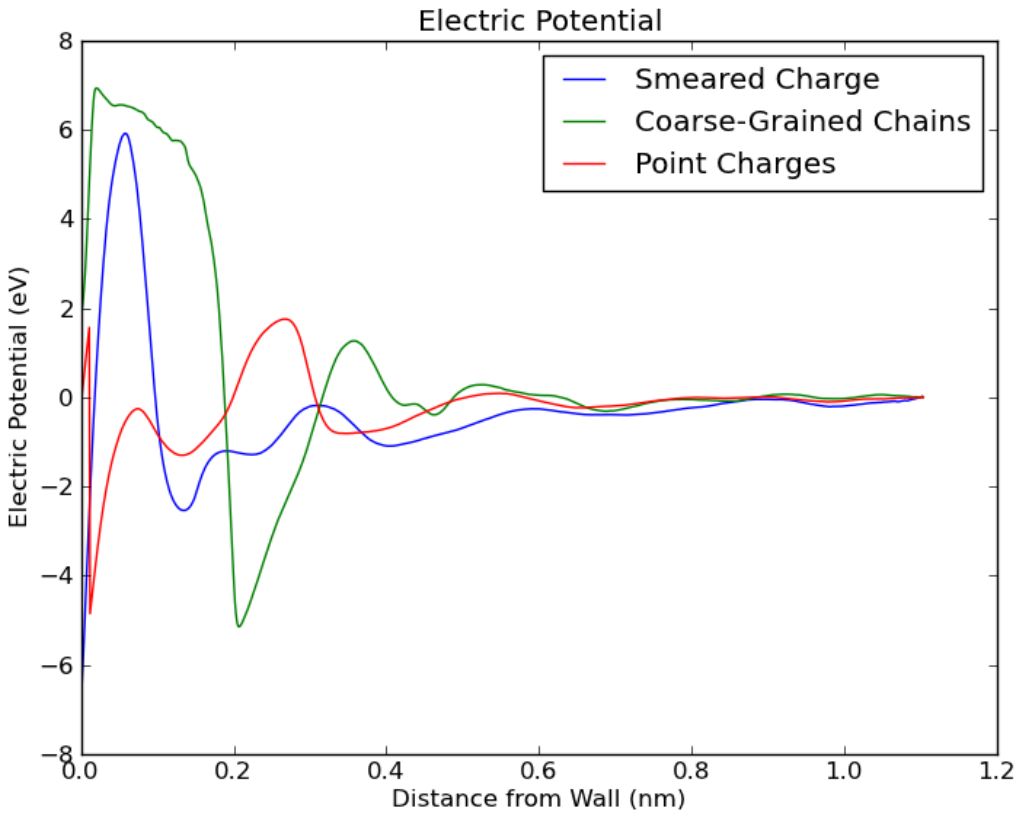

FIG. 5: Average concentration of hydronium ions as a function of distance from the pore walls for our 3 models

for 15k more steps, and the results are shown in Figures 6 and 7.

Also examined were pores of radius 1.54 nm, with λ's of 0, 1, 2, 3, 4, 5, 6 to demonstrate the effects of varying water content on the system. These were equilibrated for 15k steps and data were recorded for another 15k steps just as before, and the results are shown in Figures 8 and 9.

B. Calibration of Applied Fields

Taking our own measurements of electric potential along with those of Pintauro and Berg, it was noted that the electric fields near the walls of the cylinder were often on the order of 1eV/nm. We previously predicted that the applied electric field would need to be much smaller than 1eV/nm in order for our conductivity measurements to be accurate. In order

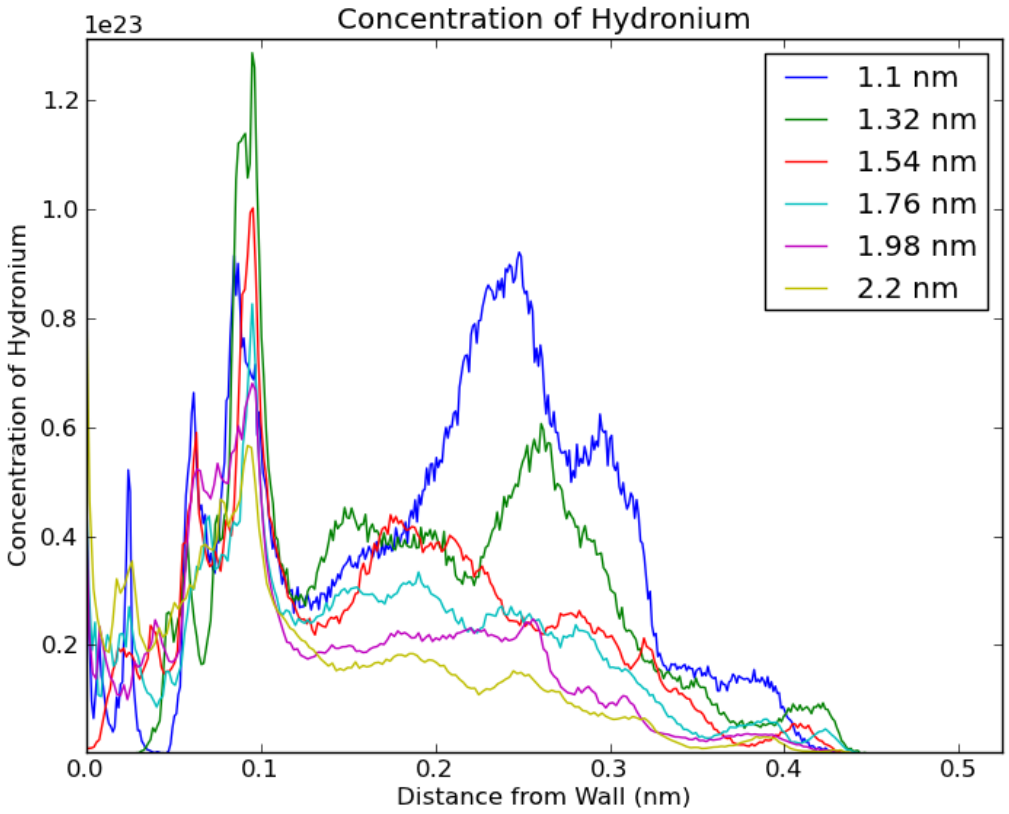

FIG. 6: Average concentration of hydronium ions as a function of distance from the pore walls for varying pore radius

to choose reasonable magnitudes of the electric field, a system was simulated with a radius of 1.1 nm and 80 hydronium ions. For this basic test, the smeared charge model was used for simplicity.

There is a relatively linear region on all the plots where the magnitude of the field is less than or equal to 0.2 eV/nm. When choosing an implied field, it is beneficial to choose a field of large magnitude in order to increase the counts of particles moving through the system and thus reduce the relative magnitude of the error in conductivity measurement. However, there is an upper limit where increasing the magnitude of the field is no longer beneficial because it results in a 50% acceptance rate of trial moves, and ohm's law no longer appears to apply. Based on Figure 10, applied fields with magnitudes less than or equal to 0.2 eV/nm should still be well within this linear region, and based on this observation, many of the fields used in the remainder of this paper will be chosen from the range of -0.2 eV/nm

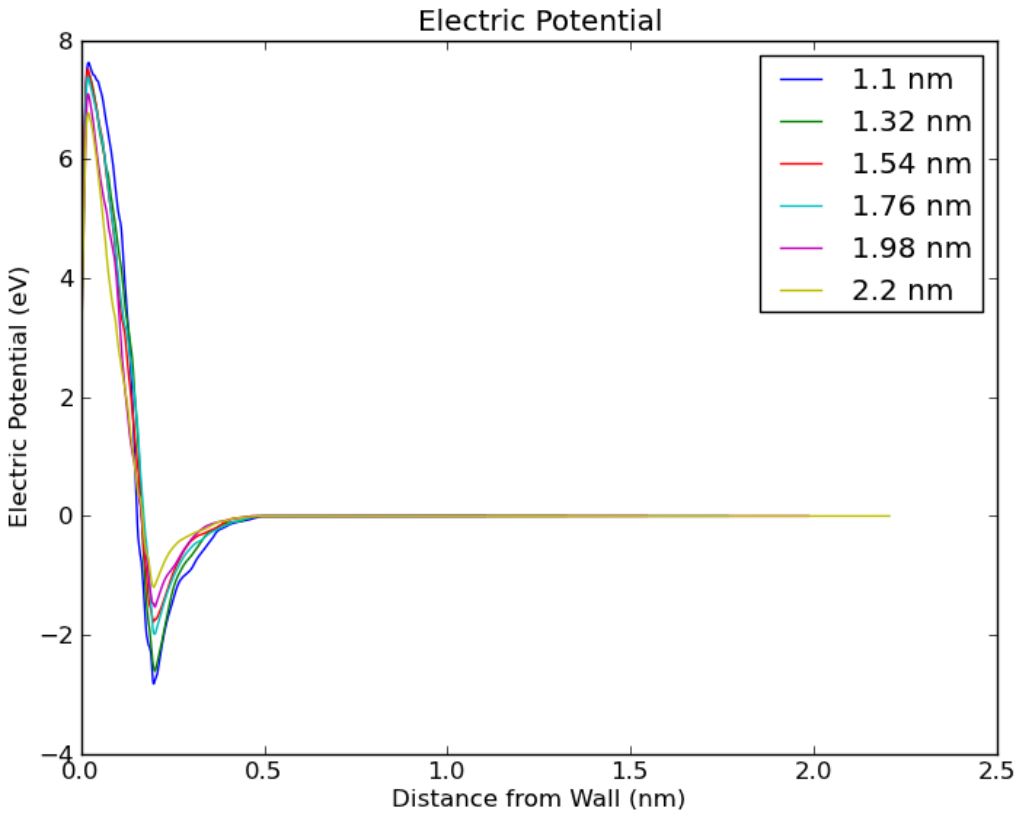

FIG. 7: Average Electric potential as a function of distance from the pore walls for varying pore radius

to 0.2 eV/nm.

C. Current Estimate

In addition to predicting the ion concentration and electric potential within a pore, Berg also predicted the pore conductivity and the ion current that results from an applied electric field. For the purpose of comparing his theoretical predictions with our 3 models, several pores were examined, each with a radius of 1.10 nm, and $\lambda = 0$. A large number of values for the applied field were tried, and the resultant currents were measured. Shown in Figure 11 is the result of those simulations.

Several simulations were examined with pore radii of 1.10 nm, 1.32 nm 1.54 nm, 1.76nm, 1.98 nm and 2.20 nm, and a constant field of 0.2 eV/nm using the coarse-grained side chain

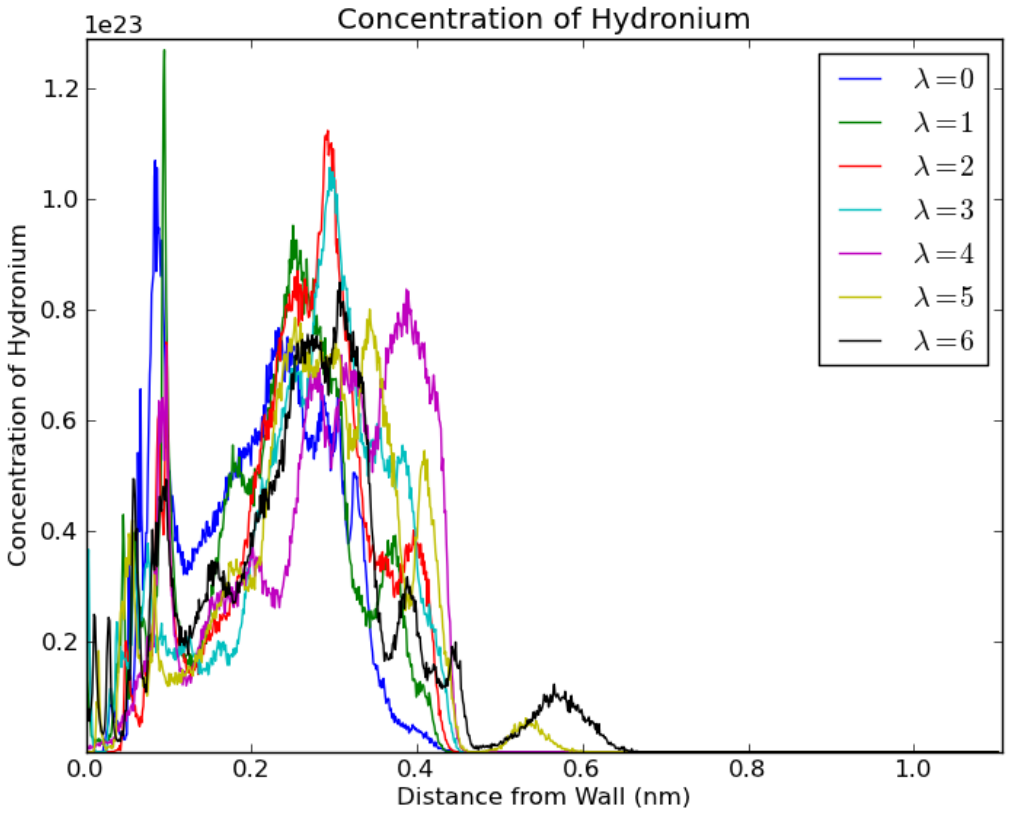

FIG. 8: Average concentration of hydronium ions as a function of distance from the walls of the pore for varying λ

model.

Several other simulations were examined with a 1.10 nm radius pore, λ's of 0, 1, 2, 3, 4, 5, 6, with a constant applied field of 3.5 eV/nm, and the coarse-grained side chain sulfonate model.

V. DISCUSSION

A. Ion Concentration and Electric Potential

It can be clearly seen in Figures 4 and 5 that the choice of sulfonate model matters a great deal to the ion concentration and electric potential measurement.

It is worth noting that we cannot compare our ion concentration measurements directly with Pintauro's because he studied ions other than hydronium, though other ions should

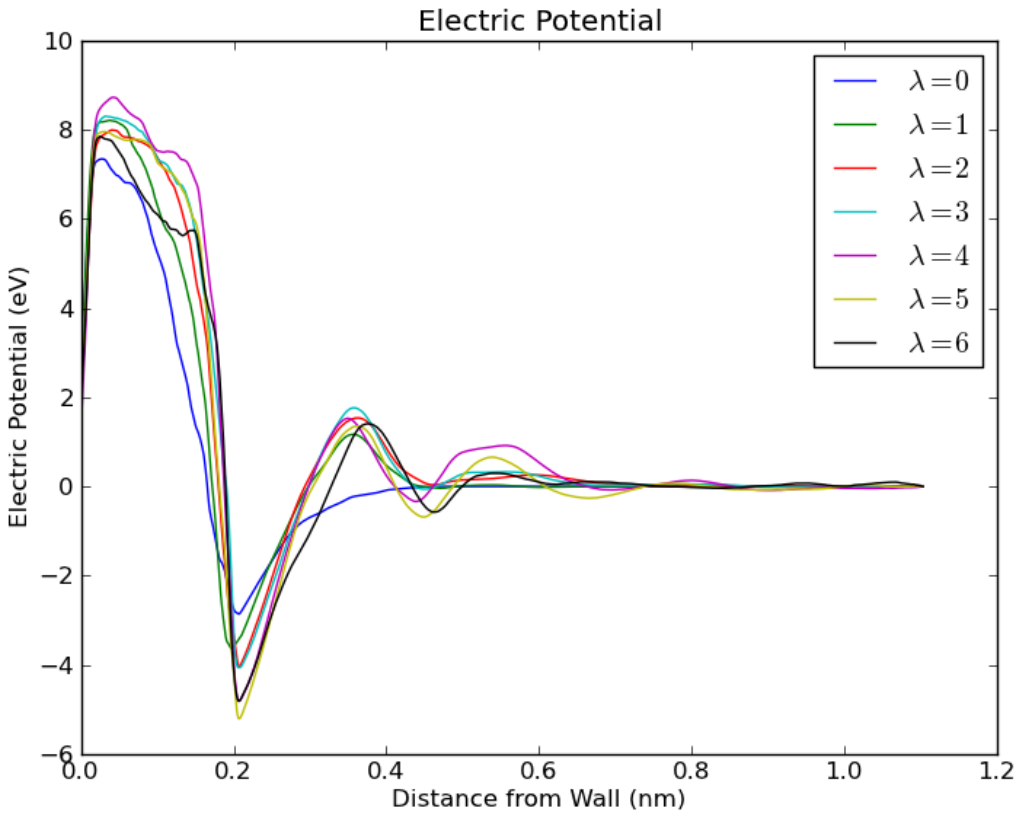

FIG. 9: Average electric potential as a function of distance from the walls of the pore for varying λ

produce qualitatively similar plots.

If we take this distance into account, we find that Berg's theory and Pintauro's simulations do indeed have a similar form to the measured values of the smeared charge model. This is to be expected because their results both ignored the existence of the sulfonate ions, just like our smeared charge model. Furthermore, this system included a no water, much like Pintauro's results and like the theory from Berg that we plotted. Pintauro assumed that the effect of water was negligible near the walls of the cylinder due to the high density of ions, which we also find to be the case in many simulations. While there are some slight differences between Pintauro's results and our results for the smeared charge model, we find that they qualitatively give the same description; that is to say, that the hydronium will only be found along the edges of the pore. Likewise, we see that the smeared charge model matches well with the work of Berg and Ladipo and also with Eikerling and Kornyshev[12].

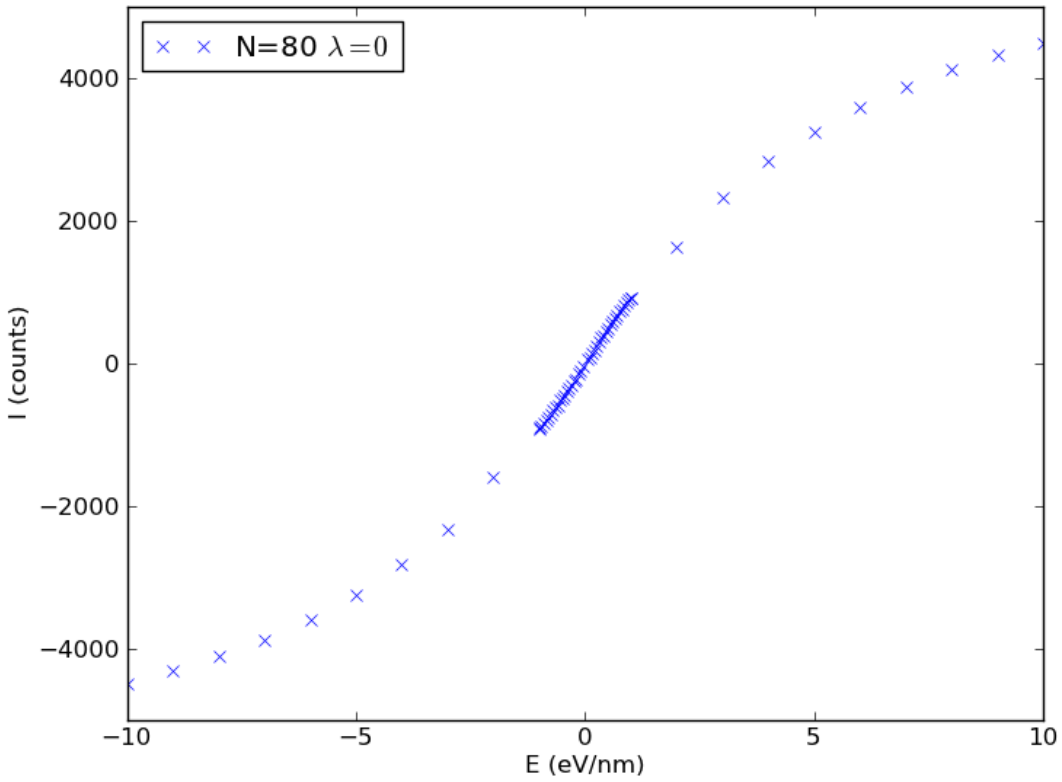

FIG. 10: Current estimate as a function of applied field magnitude for 1000000 steps

This makes an awful lot of sense because they all used the smeared charge model.

However, none of their results match well with the coarse-grained sidechains or the point charge model. One explanation is that the sulfonates in those models take up extra space on the edges of the cylinder which lowers the ion concentration on the edges of the pore. Quite simply, there is something on the sides of the pore which is not a hydronium ion and has a Lennard-Jones potential that keeps hydronium ions out of the nearby region.

Examination of the plots of electric potential for various models don't appear to yield much useful information. There are oscillations that could be explained by the positions of positive and negative charges on the hydronium and water. However, these oscillations are to be expected. Consider the simple case that some of the explicit water were in a cylinder with a radial field, much like we might expect to see in our pores. The water would tend to align in the direction of the field though there would be variation due to thermal noise. In this case, the algorithm for computing the electric field would make a large number

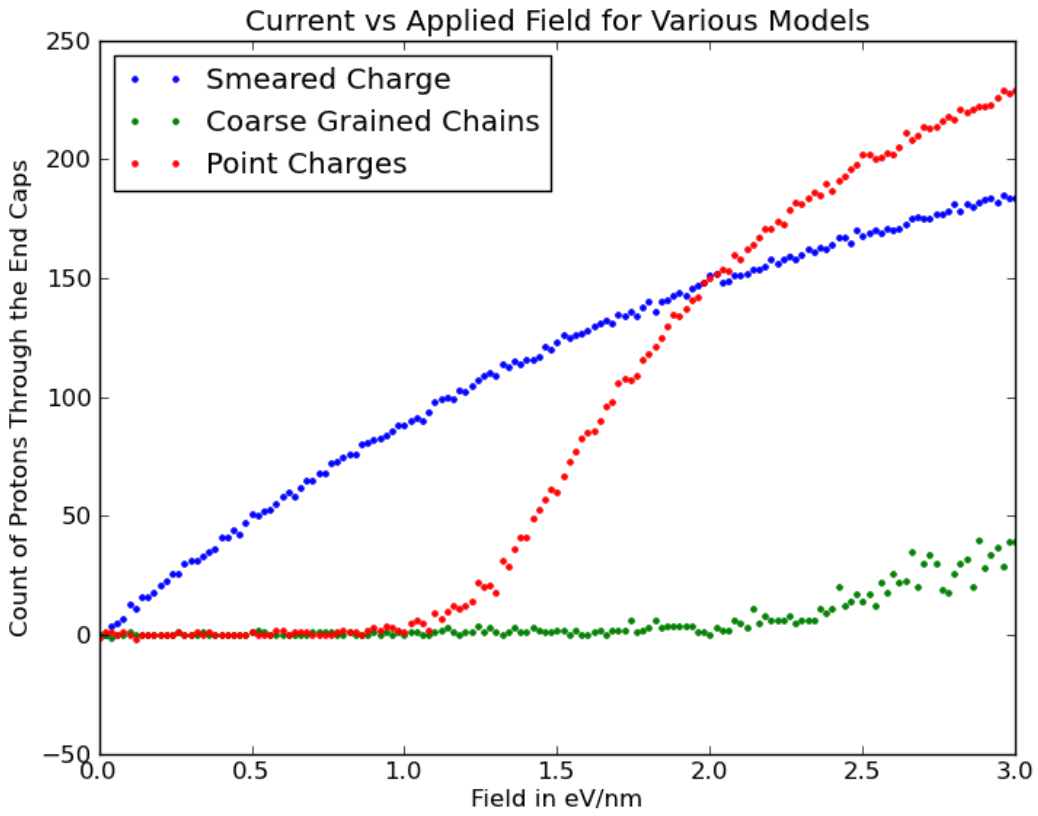

FIG. 11: Current estimate as a function of the number of hydronium ions in the system for all three sulfonate models and Berg's theory.

of bins and sum the charge contained by each bin and all of the smaller bins, and apply Gauss's laws to find the field. Since there are positive charges on the hydrogen and negative charges on the oxygen, oscillations would be expected, and would say very little about what is actually occurring within the system. None of the researchers we compared with showed these oscillations, but because they don't say much about where the constituents of the system are, it doesn't reduce the accuracy of their predictions by very much.

Also, it should be notes that the smeared charge model has a large charge imbalance for the plotted region, with the imaginary negative charges being on the outside, which is partly why it differs so greatly from the coarse-grained sidechains. When using the coarse-grained sidechains, the oxygen atom may or may not be inside the cylinder, based on the positioning of the chain and its random motion. This causes the peak near the wall of the cylinder when using the coarse-grained sidechains.

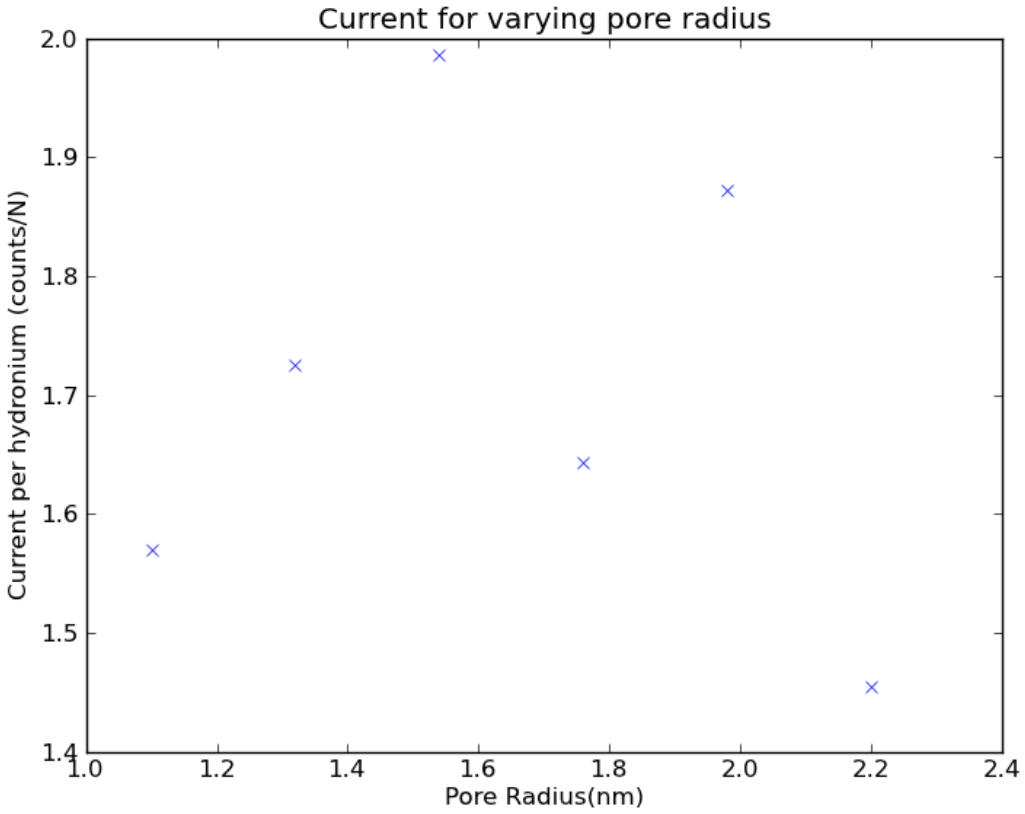

FIG. 12: Current estimate as a function of cylinder radius

With regard to the plots of ion concentration and electric potential, we had assumed that varying the radius should have some impact on the ion concentration, but that does not appear to be the case. Berg's predictions state that the ion concentration have some dependence on the pore radius, but that appears not to be a significant factor. This could have something to do with the choice of examining the coarse-grained sidechains and not the smeared charge model, as some of Berg's other predictions have already been found to be very different than the results that we find with either of our sidechain models.

Likewise, we had assumed that making significant changes to the water content, λ, would make changes in the pore's behavior by providing a dielectric constant. However, it appears that the hydronium displaces nearly all of the water near the edges of the pore, and that the dielectric constant should be very near unity. Plots of this water concentration are not shown, but it should be clear from plots of the ion concentration that there can be little to no water near the edges of the system because the concentration of hydronium is so

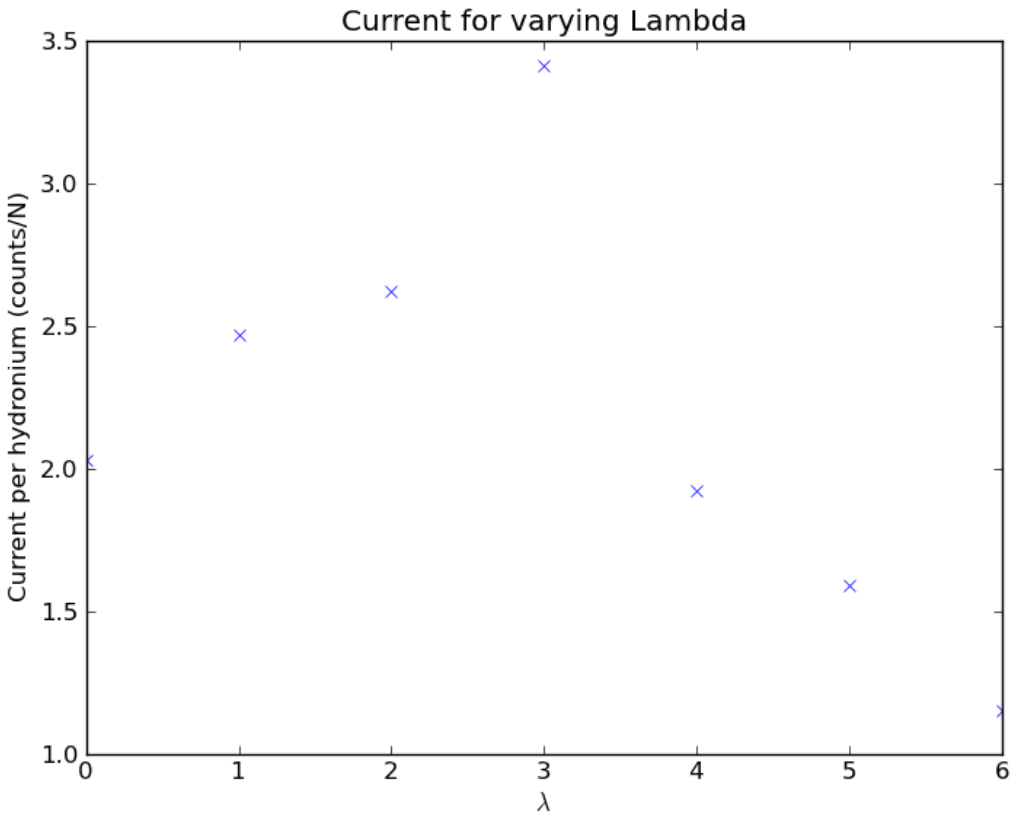

FIG. 13: Current estimate as a function of λ

high. Even when using the coarse-grained sidechains, this holds true because even if the ion concentration falls, the sidechains themselves still occupy space.

B. Current Measurement

Examination of Figure 11 clearly shows a difference in behavior based on the model that is used. The most noticeable feature is that the smeared charge model's conductivity appears to be a constant for small values of the applied field, whereas it is not a constant for the point charge model and the coarse-grained chains. For the smeared charge model, our data completely agrees with the work of Berg and Ladipo[7]. This was expected given that without the sidechains, all of the constituents of the system are free to move, and the net charge of the system would tend to make flow occur in the direction of the applied field in accordance with ohm's law.

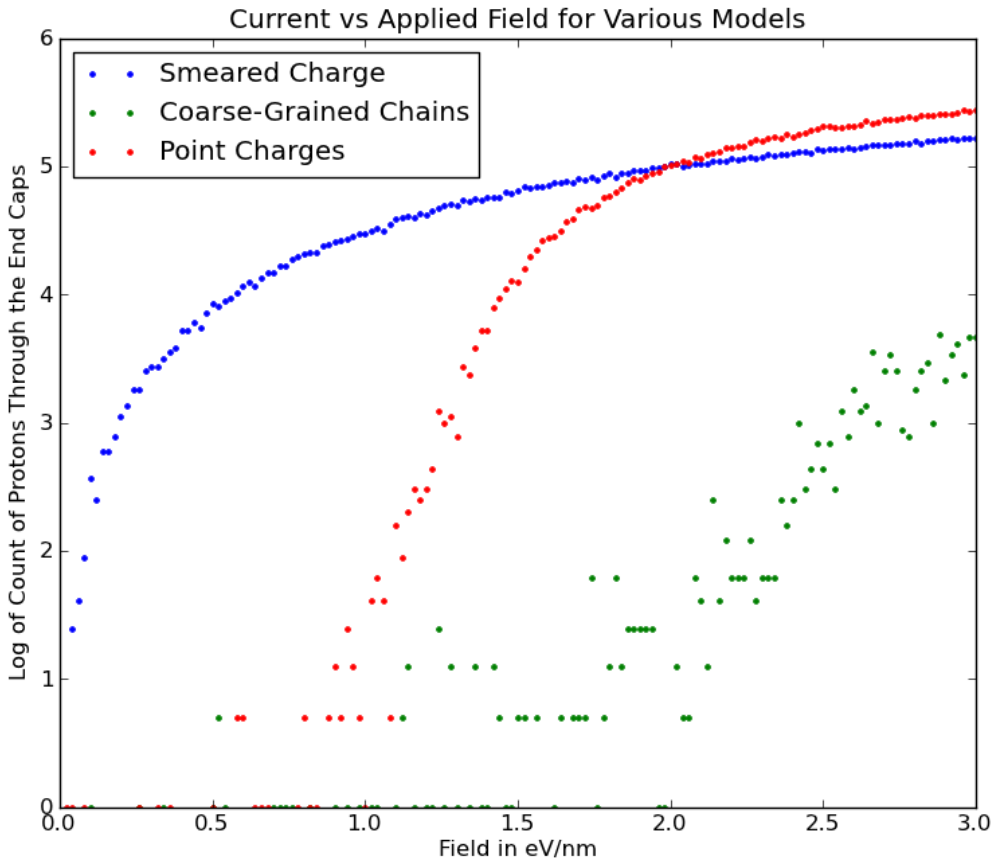

FIG. 14: Current estimate as a function of the number of hydronium ions in the system for all three sulfonate models.

However, inclusion of the more detailed sidechain models yields a completely different result. After including the coarse-grained chains or the point charges, the conductivity of Nafion no longer appeared to be a constant, and instead varied greatly with the applied field. This is much more consistent with the work of Katsaounis, et al, which experimentally found that Nafion's conductivity increased exponentially until a saturation point was reached[13]. This differers quite a bit from the results of Berg and Ladipo who treated Nafion as a conductor[7]. Shown in Figure 14 is this the logarithm of the current as a function of the applied field.

For the case where Nafion's conductivity grows exponentially until it reaches a saturation point, then it stands to reason that due to ohm's law,

$$I = \sigma E \tag{4}$$

it stands to reason that the current should go as

$$I = \alpha E e^{E/\beta} \tag{5}$$

for some α and some β until it reaches a saturation point. If that is the case, then a plot of the log of the current should go as

$$\ln I = \alpha + E + \ln \frac{E}{\beta} \tag{6}$$

until the saturation point is reached and then it will go as $\ln I = \ln \frac{E}{\beta}$. However it should be noted that the dominant term of $E + \ln \frac{E}{\beta}$ is the linear term and that to the reader, it might look just like a line, especially for large values of E. Furthermore, it should be noted that for smaller values of E, we have very little data because there little to no current, and that we can ignore α because that is just the offset of the linear region. Thus, the region where this logarithmic behavior would be visible, the region with small E, cannot be seen by the reader, and the plot should look just like a plot of

$$\ln I = E \tag{7}$$

that transitions to a plot of

$$\ln I = \ln \frac{E}{\beta} \tag{8}$$

which is exactly what we see in Figure 14.

It should also be noted that there isn't much useful data on that plot for the coarse-grained sidechains because the energy at which current became measurable was much too small. However on plots with much fewer data points, but a wider range of E, we have seen that the current when using coarse-grained sidechains responds similarly to changing current as the current when using the point charge model. Those plots were not included as they are not publication quality due to insufficient amounts of data.

For the plots of ion current as a function of pore radius and of varying λ the ion current was divided by the number of ions. This was done first on the plot of varying radius because the number of ions was larger for larger pores. This was also done with the plot of ion current as a function of λ so that the reader could easily compare with the plot of varying radius.

There is no noticeable trend in the plot of ion current for various pore radii that is distinguishable from random noise. This is something that should be investigated further

before we publish our findings. However, for a moment, we will assume the case that there is no noticeable trend in the ion current per ion as the radius varies. If that is the case, then larger pores may have a higher conductivity simply because they have more ions in them, though at this point it is speculation.

There is what appears to be a trend in the ion current, which is to say that the $\lambda = 3$ system has the highest conductivity. This also needs to be investigated further, particularly for more values of λ, however, if this result is taken with the varying pore radius result, it begins to suggest that causing the pore to swell by increasing the water content would both increase λ and increase the radius, and that for some optimal value of these two, the conductivity could be maximized. Furthermore, these results appear to indicate that the conductivity could vary by as much as a factor of 2 due to the water content changing, and by as much as a factor of 2 by the radius changing.

---

[1] S. M and Haile, Materials Today **6**, 24 (2003), ISSN 1369-7021, URL http://www.sciencedirect.com/science/article/pii/S1369702103003316.

[2] M. Fujimura, T. Hashimoto, and H. Kawai, Macromolecules **14**, 1309 (1981), http://pubs.acs.org/doi/pdf/10.1021/ma50006a032, URL http://pubs.acs.org/doi/abs/10.1021/ma50006a032.

[3] K. A. Mauritz and R. B. Moore, ChemInform **35**, no (2004), ISSN 1522-2667, URL http://dx.doi.org/10.1002/chin.200450273.

[4] W. Y. Hsu and T. D. Gierke, Journal of Membrane Science **13**, 307 (1983), ISSN 0376-7388, URL http://www.sciencedirect.com/science/article/pii/S037673880081563X.

[5] K. Schmidt-Rohr and Q. Chen, Nature Materials **7**, 75 (2008), URL http://www.ncbi.nlm.nih.gov/pubmed/18066069.

[6] J. Bontha and P. Pintauro, Chemical Engineering Science **49**, 3835 (1994), ISSN 0009-2509, URL http://www.sciencedirect.com/science/article/pii/0009250994002053.

[7] P. Berg and K. Ladipo, Proceedings of the Royal Society A: Mathematical, Physical and Engineering Science (2009), http://rspa.royalsocietypublishing.org/content/early/2009/06/10/rspa.2009.0067.full.pdf+html, URL http://rspa.royalsocietypublishing.org/content/early/2009/06/10/rspa.2009.

0067.abstract.

[8] M. Tsampas, A. Pikos, S. Brosda, A. Katsaounis, and C. Vayenas, Electrochimica Acta **51**, 2743 (2006), ISSN 0013-4686, URL http://www.sciencedirect.com/science/article/pii/S0013468605009539.

[9] E. Allahyarov and P. L. Taylor, Journal of Polymer Science Part B: Polymer Physics **49**, 368 (2011), ISSN 1099-0488, URL http://dx.doi.org/10.1002/polb.22191.

[10] W. L. Jorgensen, J. Chandrasekhar, J. D. Madura, R. W. Impey, and M. L. Klein, **79**, 926 (1983), ISSN 00219606, URL http://dx.doi.org/10.1063/1.445869.

[11] S. S. Jang, V. Molinero, T. an, and W. A. Goddard, The Journal of Physical Chemistry B **108**, 3149 (2004), http://pubs.acs.org/doi/pdf/10.1021/jp036842c, URL http://pubs.acs.org/doi/abs/10.1021/jp036842c.

[12] M. Eikerling and A. Kornyshev, Journal of Electroanalytical Chemistry **502**, 1 (2001), ISSN 1572-6657, URL http://www.sciencedirect.com/science/article/pii/S0022072800003685.

[13] A. Katsaounis, S. Balomenou, D. Tsiplakides, M. Tsampas, and C. Vayenas, Electrochimica Acta **50**, 5132 (2005), ISSN 0013-4686, ¡ce:title¿Electrochemistry: from Nanostructures to Power Plants¡/ce:title¿ ¡ce:subtitle¿Selection of papers from the 55th Annual Meeting of the International Society of Electrochemistry (ISE)19-24 September 2004, Thessaloniki, Greece¡/ce:subtitle¿, URL http://www.sciencedirect.com/science/article/pii/S001346860500530X.